

anomalous interaction radius.^{3,6,7} For example, at 200 MeV/c the interaction radius deduced from analysis of the elastic channel is ~ 3 fm. There is therefore rough agreement between the interaction radius determined in these different ways. In fact the $\bar{p}p$ elastic angular distribution is known to "antishrink" with increasing energy.⁸ This antishrinkage pattern is observed at the lowest momentum for which $\bar{p}p$ elastic scattering has been measured.^{3,6} The data presented here suggest that the radius of interaction in the annihilation also decreases with increasing energy.

One possible explanation of the presence of high partial waves in the absorption at these very low energies would be provided by direct-channel resonance dominance of the absorption process, provided high-spin resonances coupled strongly to the $\bar{p}p$ system. Such a possibility would only be consistent with the experimental data if there were a number of nearly degenerate states.

We wish to thank the alternating-gradient synchrotron staff, in particular Dr. D. Berley, and the 30-in. bubble chamber crew for their help in obtaining this exposure. We also wish to thank the scanning and measuring staff at the University of Wisconsin for their efficient work on this

experiment.

*Work supported in part by the U. S. Atomic Energy Commission under Contract No. AT(11-1)-881, COO-881-295.

¹U. Amaldi, Jr., B. Conforto, G. Fidecaro, H. Steiner, G. Baroni, R. Bizzari, P. Guidoni, V. Rossi, G. Brautti, E. Castelli, M. Ceschia, L. Chersovani, and M. Sessa, *Nuovo Cimento* **46A**, 171 (1966).

²D. Cline, J. English, D. D. Reeder, R. Terrell, and J. Twitty, *Phys. Rev. Lett.* **21**, 1268 (1968).

³J. English, thesis, University of Wisconsin, 1970 (unpublished); D. Cline, J. English, and D. D. Reeder, to be published.

⁴C. Coombes, B. Cork, W. Galbraith, G. R. Lambertson, and W. Wenzel, *Phys. Rev.* **112**, 1303 (1958).

⁵W. Rarita and P. Schwed, *Phys. Rev.* **112**, 271 (1958).

⁶R. Goldberg and R. J. Plano, to be published.

⁷In Ref. 3 the elastic data at 200 MeV/c were fitted by the form $d\sigma/dt \sim Ae^{-bt}$ with the resulting value $b = 60 \pm 15$ (GeV/c)². In the diffraction model $b = R^2/4$, where R is the interaction radius, which implies $R \sim 3$ fm.

⁸See for a recent compilation of $\bar{p}p$ data V. Barger and D. Cline, *Nucl. Phys.* **B23**, 227 (1970). In the absorption model antishrinkage is "explained" by a radius of interaction that decreases with increasing energy. At high energies the radius of interaction deduced from the elastic scattering is approximately 1 fm.

Measurement of the Reactions $\pi^+p \rightarrow K^+\Sigma^+$ and $\pi^+p \rightarrow K^+Y^{*+}$ Near Zero Degrees*

P. Kalbaci, C. W. Akerlof, P. K. Caldwell, C. T. Coffin,
D. I. Meyer, P. Schmueser,[†] and K. C. Stanfield

Harrison M. Randall Laboratory of Physics, The University of Michigan, Ann Arbor, Michigan 48104

(Received 14 May 1971)

We have measured the differential cross section for the reaction $\pi^+p \rightarrow K^+\Sigma^+$ at 3, 5, and 7 GeV/c from 0° to $\sim 3.5^\circ$ in the laboratory. The cross section at 5 and 7 GeV/c continues to 0° with an exponential t dependence consistent with data at larger angles. However, the 3-GeV/c data exhibit a change in slope near $|t| \approx 0.1$ (GeV/c)². We have also measured the differential cross section for $\pi^+p \rightarrow K^+Y^*(1385)$ at 5 GeV/c in the same angular range. These data indicate a dip at 0° as would be expected if the cross section were dominated by the helicity-flip amplitudes.

Previous experiments¹⁻⁴ have reported measurements of the differential cross section for the hypercharge exchange reactions

$$\pi^+p \rightarrow K^+\Sigma^+ \quad (1)$$

and

$$\pi^+p \rightarrow K^+Y^*(1385) \quad (2)$$

for incident pion momenta from 3.0 to 14.0 GeV/c

in the laboratory. These reactions are of interest because, in the language of Regge-pole theory, they involve the t -channel exchange of quantum numbers corresponding to mesons lying on the trajectories of $K^*(892)$ and $K^{**}(1420)$.

The structure of the differential cross section near the forward direction allows a determination of the relative size of the helicity amplitudes. A dip in the forward cross section is expected

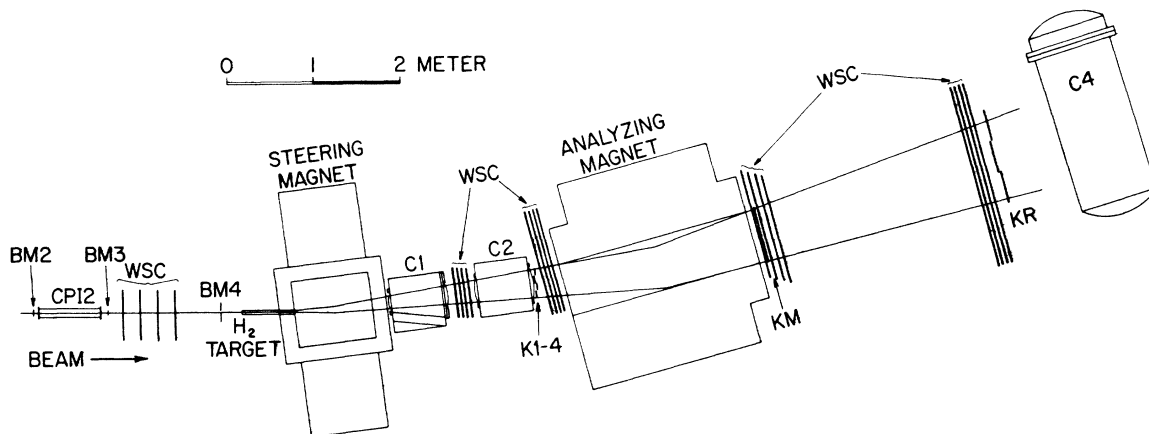


FIG. 1. A plan view of the experimental apparatus.

if the helicity-flip amplitudes dominate. Such structure, as we know from the πN charge-exchange data,⁵ would not be expected to appear except for $|t| \leq 0.15$ (GeV/c)². The experiment described here measured the differential cross section from 0° to $\sim 3.5^\circ$ for Reactions (1) and (2) in order to examine the role of the helicity-flip amplitude. It is expected that such a measurement should be a valuable constraint on current scattering theories which require varying amounts of helicity flip as compared to nonflip in order to fit the measured structure at larger t .

The apparatus is pictured schematically in Fig. 1. The momentum-analyzed beam from the zero gradient synchrotron (ZGS) struck a 24-in. long liquid-hydrogen target. Wire spark chambers with magnetostrictive readouts in the beam and the spectrometer measured the beam particle direction and the trajectory of the scattered particle through the spectrometer. The particle momenta were determined from their bend angle through the "analyzing" magnet. The purpose of the "steering" magnet is related primarily to a companion experiment in which data were accumulated on double-charge-exchange reactions. A kaon was identified in the spectrometer by a count in the threshold gas Cherenkov counter C1 and no count in C2 or C4 which were set to count pions. Similarly, a beam pion was identified by two threshold gas Cherenkov counters set to count pions. CPI 1, which was upstream of the apparatus in the beam transport system, is not pictured. The trigger was created by a pion in the incident beam followed by a kaon scattered into the spectrometer.

The experiment was connected on-line to an EMR 6050 computer. All of the spark-chamber

data as well as the status of hodoscope counters and pulse height in C1 were recorded on magnetic tape for later analysis. In addition, the data rate was such that all events were analyzed and histogrammed while the data were accumulated.

Because the acceptance of the spectrometer includes 0° , the beam also passes through the apparatus. The Cherenkov-counter requirement in the trigger was changed under computer control so that the beam was allowed to trigger the system during every tenth ZGS pulse. Analysis of these events provided us with a valuable check of the magnetic fields in the magnets as well as a check of the apparatus survey. Knowing the beam trajectory through the spectrometer allows a precise determination of the kaon production angle in the spectrometer and facilitates the calculation of the apparatus geometrical efficiency. Direct measurements of the momentum and angular resolution of the overall apparatus, including the beam, were also made possible. For example, at 3.0 GeV/c it was determined that the angular resolution was ± 3.25 mrad, the momentum resolution was $\pm 0.75\%$ and the missing-mass resolution in the region of the Σ^+ was ± 40 MeV.

Figure 2 shows the missing-mass-squared distribution at 5.0 GeV/c. Events in the Σ mass peak were binned according to the four-momentum transfer $|t|$. Corrections were then applied for K and π decay, μ contamination of the beam, nuclear absorption, spark-chamber efficiency, target-empty background, and for the geometrical detection efficiency. The geometrical acceptance of the apparatus was determined to a statistical accuracy of $\approx \pm 0.25\%$ for a Δt bin of 0.005 (GeV/c)² using the Monte Carlo technique. In addition to faithfully reproducing all cuts im-

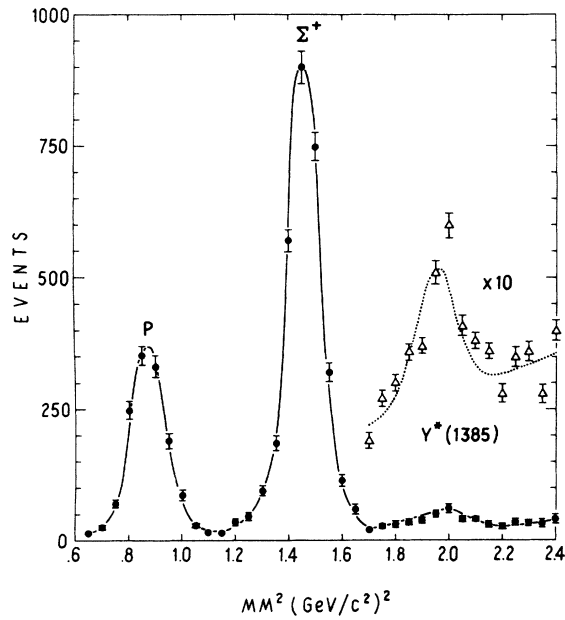


FIG. 2. Spectrum of missing-mass squared. The proton peak is due to inefficiency in vetoing beam pions and represents an overall inefficiency of $\sim 10^{-6}$. The dotted line is a best fit to the Y^* region as described in the text.

posed by the on-line program, the Monte Carlo program included effects due to multiple Coulomb scattering, beam-spot size (± 0.28 in. horizontally, ± 0.22 in. vertically), beam angular divergence (± 5.3 mrad vertically, ± 3.4 mrad horizontally), and beam-momentum resolution. The angular divergence and momentum resolution of the beam are measured directly as discussed above and the measured distributions are used in the Monte Carlo calculation.

The data are presented in Table I. The errors indicated are statistical only; we estimate the systematic uncertainty of these results to be $\lesssim \pm 10\%$. In Fig. 3 we compare the $\pi^+p \rightarrow K^+\Sigma^+$ results of the present experiment with the data of Ref. 1. The straight lines are best fits of the form $A \exp\{B(t-t_{min})\}$. At 5.0 and 7.0 GeV/c the differential cross section continues to 0° with a slope consistent with the previous data. However, at 3.0 GeV/c the cross section falls more rapidly from $|t_{min}|$ to $|t| \approx 0.1$ than at larger angles. At all energies we have included data from both experiments in the exponential fits. For the purpose of these fits the 3.0-GeV/c data were separated into two regions divided by $|t|$

Table I. $d\sigma/dt$ in μb $(\text{GeV}/c)^{-2}$ for Reactions (1) and (2), and best fits to Eq. (3).

$\pi^+p \rightarrow K^+\Sigma^+$			$\pi^+p \rightarrow K^+Y^*$				
3.0 GeV/c		5.0 GeV/c		7.0 GeV/c		5.0 GeV/c	
$ t $	$d\sigma/dt$	$ t $	$d\sigma/dt$	$ t $	$d\sigma/dt$	$ t $	$d\sigma/dt$
.0291	685 ± 34	.0246	405 ± 17	.030	229 ± 12	.0365	7.9 ± 5.5
.0331	672 ± 40	.0446	312 ± 18	.070	153 ± 11	.0515	10.7 ± 6.4
.0381	619 ± 33	.0646	305 ± 20	.110	112 ± 10	.072	28.8 ± 6.6
.0441	543 ± 38	.0846	220 ± 20	.150	67 ± 8	.099	27.0 ± 6.5
.0511	486 ± 32	.1046	183 ± 18			.132	24.7 ± 5.7
		.1246	170 ± 18				
4.83 GeV/c $\pi^-p \rightarrow \pi^0n$ (Ref. 7)							
$A_{nf} = 21.4 \pm 1.5$		$A_{nf} = 20.3 \pm 0.3$		$A_{nf} = 16.4 \pm 0.4$		$A_{nf} = 3.03 \pm 0.75$	
$A_f = 192 \pm 20$		$A_f = 0.0 \pm 35.0$		$A_f = 40.0 \begin{smallmatrix} + 20.0 \\ - 40.0 \end{smallmatrix}$		$A_f = 35.67 \pm 5.33$	
$B = 12.0 \pm 0.6$		$B = 9.4 \pm 0.8$		$B = 10.3 \pm 1.1$		$B = 6.4 \pm 1.0$	
$\sigma_f/\sigma_{nf}^* = 1.8 \pm 0.5$		$\sigma_f/\sigma_{nf} = 0.00 \pm 0.08$		$\sigma_f/\sigma_{nf} = 0.15 \begin{smallmatrix} +0.19 \\ -0.15 \end{smallmatrix}$		$\sigma_f/\sigma_{nf} = 4.8 \pm 2.8$	

^a σ_f and σ_{nf} are the integrated cross sections as described in the text.

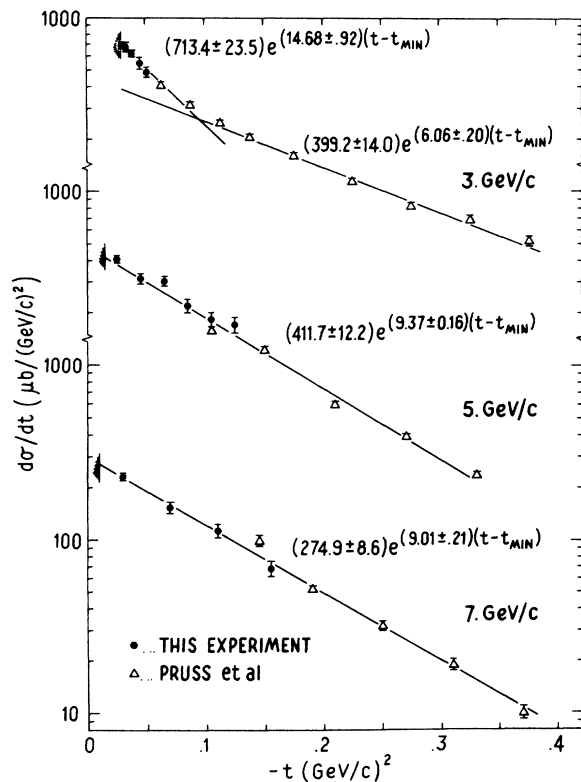


FIG. 3. Differential cross section for the reaction $\pi^+p \rightarrow K^+\Sigma^+$.

= 0.1. We have found no quantitative explanation of the structure in the 3.0-GeV/c cross section. However, at 3.0 GeV/c the total center-of-mass energy is 2.56 GeV. This is quite near the mass of several states [e.g., $\Delta(2420)$, $\Delta(2850)$] which may decay into ΣK . It is therefore possible that the structure is due to the proximity of these s-channel poles.

In addition to the procedure described above for the analysis of the $K^+\Sigma^+$ final state it was necessary to separate the Y^* from a nonresonant background. The data were divided into five angular bins of 0.7° . For each bin the mass distribution was fitted by a resonant contribution plus a flat noninterfering background. There were only three parameters to be determined: the amplitude of the resonant contribution (assumed to be Gaussian) and the amplitude and slope of the background. The mass resolution and calibration of the spectrometer were determined directly from the Σ data and the position and width of the $Y^*(1385)$ were fixed at their known values. The data for $\pi^+p \rightarrow K^+Y^*$ are compared to the results of Ref. 3 in Fig. 4.

In sharp contrast to the $K^+\Sigma^+$ data, the K^+Y^*

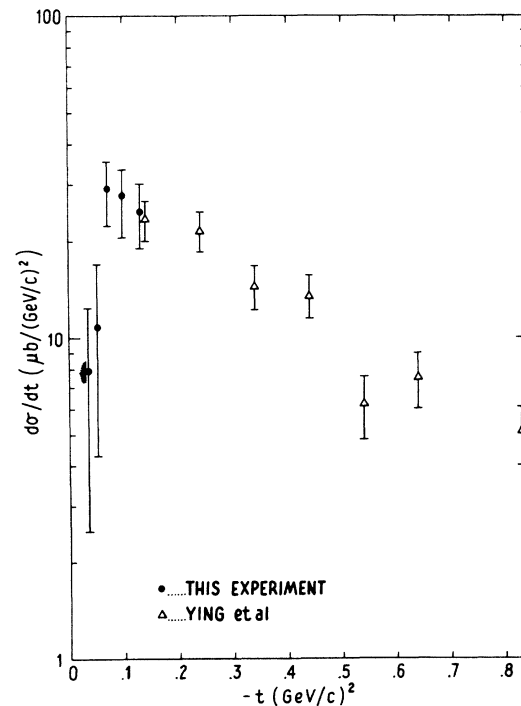


FIG. 4. Differential cross section at 5.0 GeV/c for the reaction $\pi^+p \rightarrow K^+Y^*$.

cross section shows a dip in the forward direction. This is not completely surprising since a t -channel SU(3) analysis³ relates K^+Y^* production to $\pi^0\Delta^{++}(1238)$, $\eta^0\Delta^{++}$, and $K^0\Delta^{++}$ production. Each of these cross sections is known to show a turnover in the forward direction.⁵ It is perhaps more difficult to reconcile this dip with the $K^+\Sigma^+$ data which do not show a dip although the same trajectories contribute. The answer may lie in the complexities introduced by the two different octet couplings (f/d ratio) at the $K^*N\Sigma$ vertex as compared to only one at the K^*NY^* vertex. Quantitative comparisons are made difficult by the added complexity of the Y^* case because there are three helicity-flip amplitudes as compared to only one for Σ^+ production.

The ρ -photon analogy of Stodolsky and Sakurai⁶ in $\pi\Delta$ production in πp collisions suggests that the $\rho N\Delta$ vertex is dominated by the magnetic-dipole ($M1$) transition. The observed density-matrix elements of the Δ -decay angular distribution support this hypothesis. Furthermore, the values for the density-matrix elements for $\pi^+p \rightarrow \eta^0\Delta^{++}$ are consistent with the corresponding elements for the $\pi\Delta$ case. SU(3) then suggests that similar behavior might be expected at the K^*NY^* and $K^{**}NY^*$ vertices. For the

$M1$ transition the virtual ρ (K^*) helicity state is restricted to ± 1 . In the forward direction, conservation of angular momentum at the $\pi\pi\rho$ (πKK^*) vertex requires the differential cross section for pure $M1$ amplitudes to vanish. We might therefore expect the differential cross section for Reaction (2) to behave as $|t'|A \exp(-B|t'|)$, where $t' = t - t_{\min}$. In order to get a quantitative estimate of the ratio of helicity flip to nonflip allowed by our data we have made a least-squares fit to the differential cross sections for Reactions (1) and (2) by the form

$$\frac{d\sigma}{dt} = \left[|A_{\text{nf}}|^2 + \frac{|t'|}{4M^2} |A_{\text{f}}|^2 \right] e^{-B|t'|}, \quad (3)$$

where M is the nucleon mass. The results of the best fits are presented in Table I. To understand better the significance of the fitted amplitudes we integrated the flip and nonflip contributions to the cross section over the interval $|t_{\min}| \leq t \leq 0.4$ (GeV/c)² using Eq. (3). The ratios of these contributions are denoted $\sigma_{\text{f}}/\sigma_{\text{nf}}$ and are also shown in Table I. For the $K^+\Sigma^+$ data this ratio is consistent with zero with an upper limit of 8% at 5.0 GeV/c and 34% at 7.0 GeV/c . In contrast the $\sigma_{\text{f}}/\sigma_{\text{nf}}$ ratio for the K^+Y^* channel is 4.8 ± 2.8 . Thus the $K^+\Sigma^+$ reaction is strongly dominated by the nonflip amplitude while the K^+Y^* reaction is dominated by the flip amplitudes. For comparison the data⁷ for the charge-exchange reaction have been similarly fitted and yield a ratio for $\sigma_{\text{f}}/\sigma_{\text{nf}}$ of 1.8 ± 0.5 .

We would like to thank Dr. David Rust and Dr. Drasko Yovanovitch for technical assistance and helpful discussions. We also thank Dr. Frank Henyey, Dr. Gordon Kane, and Dr. Y. P. Yao for several stimulating discussions. The staff of the ZGS at Argonne National Laboratory also deserve thanks for their support throughout

the course of the experiment.

*Research supported by the U. S. Atomic Energy Commission.

†Present address: University of Hamburg, Hamburg, West Germany.

¹S. M. Pruss, C. W. Akerlof, D. I. Meyer, S. P. Ying, J. Lales, R. A. Lundy, D. R. Rust, C. E. W. Ward, and D. D. Yovanovitch, *Phys. Rev. Lett.* **23**, 189 (1969).

²A. Bashian, G. Finocchiaro, M. L. Good, P. D. Grannis, O. Guisan, J. Kirz, Y. Y. Lee, R. Pittman, G. C. Fischer, and D. D. Reeder, to be published; J. Kirz, in *High Energy Collisions*, edited by C. N. Yang *et al.* (Gordon and Breach, New York, 1969); W. R. Butler, UCRL Report No. UCRL 19845, 1970 (unpublished); G. C. Fischer, thesis, University of Wisconsin, 1970 (unpublished).

³S. P. Ying, C. W. Akerlof, D. I. Meyer, S. M. Pruss, J. Lales, R. A. Lundy, D. R. Rust, C. E. W. Ward, and D. D. Yovanovitch, *Phys. Lett.* **30B**, 289 (1969).

⁴Bashian *et al.*, Ref. 2; W. R. Butler, UCRL Report No. UCRL 19845, 1970 (unpublished); M. Aderholz *et al.*, *Nucl. Phys.* **B7**, 111 (1968).

⁵For representative data and references to other work see $\pi^+p \rightarrow \pi^0n$, M. A. Wahlig and I. Mannelli, *Phys. Rev.* **168**, 1515 (1968); $\pi^+p \rightarrow \pi^0\Delta^{++}$, G. Gidal, G. Borreani, D. Grether, F. Lott, R. W. Birge, S. Y. Fung, W. Jackson, and R. Poe, *Phys. Rev. Lett.* **23**, 994 (1969); $\pi^+p \rightarrow \eta^0\Delta^{++}$, D. F. Grether, G. Borreani, and G. Gidal, UCRL Report No. UCRL 19778, 1970 (unpublished); $K^+p \rightarrow K^0\Delta^{++}$, Y. Goldschmidt-Clermont, V. P. Henri, B. Jongejans, A. Moisseev, F. Muller, J. M. Perreau, A. Prokes, V. Yarba, W. De Baere, J. Debaisieux, P. Dufour, F. Grard, J. Heughebaert, L. Pope, P. Peeters, F. Verbeure, and R. Windmolders, *Nuovo Cimento* **46A**, 539 (1966).

⁶L. Stodolsky and J. J. Sakurai, *Phys. Rev. Lett.* **11**, 90 (1963).

⁷P. Sonderegger, J. Kirz, O. Guisan, P. Falk-Vairant, C. Bruneton, P. Borgeaud, A. V. Stirling, C. Carverzasio, J. P. Guiland, M. Yvert, and B. Amblard, *Phys. Lett.* **20**, 75 (1966).